

1 **Understanding Controlling Factors of Extratropical Humidity**
2 **and Clouds with an Idealized General Circulation Model**

3 Michelle E. Frazer*

4 *Program in Atmospheric and Oceanic Sciences, Princeton University, Princeton, New Jersey*

5 Yi Ming

6 *NOAA/Geophysical Fluid Dynamics Laboratory, Princeton, New Jersey*

7 **Corresponding author:* Michelle E. Frazer, mefrazer@princeton.edu

ABSTRACT

8 This paper examines the physical controls of extratropical humidity and clouds by isolating the
9 effects of cloud physics factors in an idealized model. The Held-Suarez dynamical core is used
10 with the addition of passive water vapor and cloud tracers, allowing cloud processes to be explored
11 cleanly. Separate saturation adjustment and full cloud scheme controls are used to consider the
12 strength of advection-condensation theory. Three sets of perturbations to the cloud scheme are
13 designed to test the model's sensitivity to the physics of condensation, sedimentation, and precip-
14 itation formation. The condensation and sedimentation perturbations isolate two key differences
15 between the control cases. First, the sub-grid-scale relative humidity distribution assumed for the
16 cloud macrophysics influences the location and magnitude of the extratropical cloud maxima, lim-
17 iting isentropic transport of tropical moisture to the polar troposphere. Second, within the model's
18 explicit treatment of cloud microphysics, re-evaporation of hydrometeors moistens and increases
19 clouds in the lower troposphere. In contrast, microphysical processes of precipitation formation
20 (specifically, the ratio of accretion to autoconversion) have negligible effects on humidity, cloudi-
21 ness, and precipitation apart from the strength of the large-scale condensation and formation cycle.
22 Additionally, counterintuitive relationships—such as cloud condensate and cloud fraction respond-
23 ing in opposing directions—emphasize the need for careful dissection of physical mechanisms. In
24 keeping with advection-condensation theory, circulation sets the patterns of humidity, clouds, and
25 precipitation to first order, with factors explored herein providing secondary controls. The results
26 substantiate the utility of such idealized modeling and highlight key cloud processes to constrain.

27 **1. Introduction**

28 Cloud feedback is widely considered to be the largest contributor to the intermodel spread in
29 climate sensitivity among comprehensive General Circulation Models (GCMs) (e.g., Ceppi et al.
30 2017; Sherwood et al. 2020). Bony et al. (2015) argued that consensus among most comprehensive
31 GCMs does not, on its own, yield robust conclusions on cloud feedback. Rather, theories which
32 underpin physical arguments and improve understanding in a way that allows for expanded use
33 and interpretation of comprehensive GCMs are an additional requirement. Thus, simple models
34 whose workings can be clearly grasped play a key role in the midst of a complex scientific problem
35 (Pierrehumbert et al. 2007; Held 2005, 2014). If a GCM produces both observationally-constrained
36 cloud fields and multi-model consistent cloud feedbacks, but without the physical mechanisms
37 necessarily being represented appropriately, its prediction of the climatic response to a radiative
38 forcing may be significantly flawed. With the potential for unrealistic interactions between different
39 parameterized processes (Ceppi et al. 2017), decomposition of the effects of individual processes
40 could lead to improved parameterizations.

41 Here, we study under-constrained cloud macrophysical and microphysical processes by exploring
42 the underlying physical mechanisms. Since changing a stratiform cloud scheme can have significant
43 ramifications, even reversing a model's feedback with warming (Geoffroy et al. 2017), we use an
44 idealized setup to break down a cloud scheme and understand the effects of individual cloud
45 processes on atmospheric humidity and cloudiness. The processes studied herein are motivated by
46 three factors: understanding the differences between the advection-condensation theory of humidity
47 and a cloud scheme, the controls of precipitation efficiency, and the direct effect of stratiform-cloud
48 related GCM parameters on free tropospheric humidity and clouds.

49 *a. Advection-Condensation Theory*

50 Free tropospheric humidity is important to the distribution of clouds and precipitation. The
51 so-called advection-condensation theory suggests that water vapor (WV) in the atmosphere is most
52 simply reflective of the lowest temperature (lowest saturation specific humidity) experienced by
53 the parcel since leaving the nearly saturated surface layer. This theory alone can describe WV
54 distribution to first order (Sherwood et al. 2010). Advection-condensation theory helps explain
55 two key features of free tropospheric humidity: dry subtropical zones and moist polar regions
56 connected by dry isentropes.

57 Pierrehumbert (1998) laid out three factors which contribute to the dry subtropics. First, sub-
58 sidence brings down dry air, and would keep the region at the mixing ratio of the tropopause if
59 not for other mechanisms. Second, lateral mixing brings in moist air from the tropical convective
60 region. Third, processing of air through cold extratropics dries the region. Thus, the dry subtropics
61 and moist poles are connected through nearly isentropic large-scale advection, and cycling through
62 cold polar upper tropospheric air is a key means of dehydrating air in the extratropics (Kelly et al.
63 1991). Finally, Pierrehumbert (1998) also noted the role of re-evaporation of hydrometeors as
64 a subtropical moisture source as emphasized by Sun and Lindzen (1993), but suggested this is
65 limited by weak rainfall. Also suggesting the importance of in situ moistening processes in the
66 midlatitudes, Yang and Pierrehumbert (1994) showed that in the advection-condensation model,
67 the tropical moisture source is too inefficient (that is, too weak of mixing between tropics and
68 extratropics). These factors have been expounded in further work.

69 Using a simple saturation adjustment scheme as a representation of advection-condensation the-
70 ory, Galewsky et al. (2005) found that the primary dynamical control of the dry subtropics was
71 isentropic dehydration by mid-latitude eddies (with diabatic descent through Hadley circulation

72 playing a secondary role). WV is transported from the lower deep tropics to the upper polar extrat-
73 ropics by baroclinic eddies along isentropes, with the moist air rising and cooling adiabatically. The
74 storm tracks interrupt the transport such that significant moisture is released through precipitation
75 before reaching the poles. Thus, the return flow supplies dehydrated air to the subtropics, and is
76 confined to isentropic layers (Held and Schneider 1999). The poleward eddy WV transport follows
77 dry isentropes but different values of equivalent potential temperature, with this moist recirculation
78 peaking on the equatorward side of the storm tracks (Laliberté et al. 2012). In this study, we
79 consider how a cloud scheme distributes moisture differently than simple saturation adjustment (as
80 in Galewsky et al. 2005), and we highlight the processes—cloud macrophysics and microphysics
81 alike—that affect extratropical humidity strongly. The physical mechanisms of these controls are
82 delineated to highlight those processes that need to be represented accurately in cloud schemes.

83 *b. Precipitation Efficiency Controls*

84 Differences between saturation adjustment and a cloud scheme are closely related to the con-
85 trols of precipitation efficiency. The residence time of water in the atmosphere is, in a full cloud
86 scheme, affected by three efficiencies: the efficiency with which WV may become cloud conden-
87 sate (condensation), become part of a falling hydrometeor (formation), and reach the surface as
88 precipitation (sedimentation) (Langhans et al. 2015). Advection-condensation theory reduces this
89 complexity to one efficiency since WV in excess of saturation immediately becomes surface pre-
90 cipitation. Thus, condensation and sedimentation efficiencies highlight two of the key differences
91 between a saturation adjustment scheme (based on advection-condensation theory) and a full cloud
92 scheme (closer to reality): condensation efficiency is affected by assumptions of small (sub-grid)
93 scale RH distribution, and sedimentation efficiency by re-evaporation of precipitation. The third
94 efficiency—formation efficiency—can be affected by internal cloud scheme parameters such as the

95 assumed cloud condensation nuclei (which affects warm rain processes) or the fall speed of ice.
96 But each of the three efficiencies have the potential to significantly affect WV and cloud condensate
97 (CC) fields, the distribution of precipitation, and the overall residence time of atmospheric water.
98 For example, precipitation efficiency (the multiplicative product of formation and sedimentation
99 efficiencies; see section 2b) is frequently highlighted as being potentially affected by creating more
100 liquid at the expense of ice in mixed-phase clouds (Klein et al. 2009; McCoy et al. 2015; Ceppi
101 et al. 2016; McCoy et al. 2018). Here we explore the direct effect of changing these efficiencies on
102 steady-state fields which are relevant to radiative feedbacks.

103 *c. GCM Stratiform Tuning Parameters*

104 Thus the first two motivations are connected to the third of the direct effect of stratiform-cloud
105 related GCM tuning parameters on free tropospheric humidity and clouds. Critical RH (the
106 minimum GCM grid-box-mean RH needed for cloud condensate formation) is a useful tuning
107 parameter for radiative balance (through shortwave cloud radiative effects), but may be tuned
108 artificially high in order to compensate for too-bright clouds (McCoy et al. 2016). Critical RH is
109 important because it controls large-scale condensation, a sink of WV and source of CC. WV can
110 be altered without directly affecting CC by tuning the re-evaporation of precipitation. Another key
111 parameter is N , the assumed cloud drop number concentration: aerosols affect microphysics and
112 thus precipitation and radiation through aerosol-cloud interactions. The observed precipitation rate
113 can be expressed as a power-law function of LWP and N , with a strong correlation between LWP
114 and the ratio of accretion to autoconversion processes (hereafter $accr/auto$; Jiang et al. 2010). At
115 low LWP, $accr/auto$ is small because of few generated rain drops. Some GCMs directly model
116 aerosol indirect effects, but even in simpler cloud microphysics schemes which lack an explicit
117 representation of aerosol indirect effects, the autoconversion process is a direct function of N

118 and thus a major control of $accr/_{auto}$, which is a key parameter for examining the balance of
119 microphysical conversion processes from cloud water to rainwater (e.g., Gettelman et al. 2013).

120 In a GCM study implementing five different autoconversion schemes, Michibata and Takemura
121 (2015) found significant variance in $accr/_{auto}$. But, these schemes showed a commonality of
122 the relative role of the accretion process being one or more orders of magnitude underestimated
123 compared to observations (as estimated by Gettelman et al. 2013). This incorrect ratio comes
124 from both too high simulated autoconversion rates (Gettelman et al. 2013, 2014) and in some
125 schemes, too low of an accretion enhancement factor for correct precipitation intensity (Wu et al.
126 2018). The high simulated autoconversion rates come from diagnostic precipitation which forms
127 warm rain too easily (Jing et al. 2017). Cloud condensation nuclei and $accr/_{auto}$ affect not only
128 precipitation rates but also radiative forcing. Gettelman et al. (2013) noted a strong increase in
129 LWP with simulated $accr/_{auto}$ (as in observations), and cloud optical depth and thus shortwave
130 radiative effect is significantly controlled by LWP (e.g., Stephens 1978). As past studies have likely
131 underestimated the true sensitivity of clouds and radiation to aerosols, the negative forcing of the
132 Twomey effect (altered cloud albedo from increased anthropogenic aerosols) may be underestimated
133 (Quaas et al. 2020). Yet, Gettelman et al. (2013) suggested that the autoconversion rate bias can be
134 corrected by altering the relative balance of the autoconversion and accretion rates, which lowers
135 the radiative effect of aerosol cloud interactions. Thus, understanding the interplay and impacts of
136 altered N and $accr/_{auto}$ is critical.

137 *d. Purpose and Organization*

138 The overarching purpose of this paper is to employ an idealized model setup to shed light on what
139 controls free tropospheric humidity and cloudiness. Using perturbation experiments which isolate
140 key processes, we aim at elucidating the complex connections among WV, clouds, precipitation,

141 and circulation. In analyzing the control and perturbation experiments in this study, the budgetary
142 terms of the cloud scheme which represent the conversions among WV, CC, and precipitating
143 water (P) are particularly emphasized. This method is motivated by a need for a robust physical
144 understanding to ground model representations of cloud processes in order to lend confidence to
145 model-inferred relationships (Shepherd 2014; Stevens and Bony 2013).

146 A process-based analysis is related to the secondary purpose of this work: to clearly demonstrate
147 the value of this modeling tool (a dry GCM with passive water and cloud tracers) for developing a
148 systematic understanding of physical controls on humidity and clouds and diagnosing their repre-
149 sentations in models. This approach is in the same spirit as “mechanism-affirmation experiments”
150 described in Jeevanjee et al. (2017) as being the provision of a model hierarchy framework. In
151 terms of the model hierarchy, the setup used in this paper (Ming and Held 2018) is derived from the
152 Held-Suarez (HS) dry GCM, but in a different direction than the Frierson moist aquaplanet GCM
153 (Frierson et al. 2006) which extended the HS dry GCM by adding a gray radiation scheme and moist
154 physics such that latent heating affects the model’s dynamics. Our model is in many aspects more
155 idealized than the Frierson model with dry dynamics and no radiation scheme, but more complex
156 in its addition of a full cloud microphysics scheme. It can be thought of as one rung higher on the
157 model hierarchy ladder than the HS dry GCM, but one rung lower than the Frierson model. This
158 setup is therefore uniquely suitable for answering specific questions about extratropical humidity
159 and cloudiness—namely the direct effects of cloud macrophysics and microphysics—as well as the
160 physical mechanisms behind these effects.

161 This paper is organized as follows. Section 2 lays out the methodology of this study, describing
162 the idealized model, experiments, and analysis framework. Section 3 describes the results from the
163 control saturation adjustment and cloud physics experiments and the condensation, sedimentation,
164 and formation perturbations. Section 4 discusses the implications of these results for the value of

165 the advection-condensation paradigm, key stratiform cloud physics processes to constrain, and the
166 utility of this idealized model.

167 **2. Methodology**

168 *a. Control Models*

169 The idealized model used here is based on the HS dry GCM (Held and Suarez 1994) with the
170 addition of four passive water and cloud tracers—specific humidity, cloud liquid, cloud ice, and
171 cloud fraction (CF)—as described in Ming and Held (2018). The dry GCM uses a hydrostatic
172 spectral dynamical core for an ideal gas atmosphere with no topography. For this work, a resolution
173 of T42 (referring to the maximum number of zonal waves present in the triangular truncation) is
174 used, resulting in a horizontal grid of 128 by 64 cells (about 2.8° spacing) with 20 vertical layers
175 equally spaced in the sigma coordinate. The forcing consists of Newtonian relaxation of temperature
176 toward a prescribed zonally symmetric equilibrium temperature and planetary boundary layer drag
177 represented by Rayleigh damping. This idealized setup enables the isolation of the roles of various
178 cloud processes. It assumes that latent heating or cooling from conversions among WV, CC, and
179 precipitation do not feed back on the dynamics. Also, with no explicit radiation scheme in the
180 model, clouds do not affect circulation through cloud radiative effects. Thus, WV and clouds are
181 passive in that they do not affect circulation or temperature patterns.

182 Two control simulations are created with results explored in section 3a. The first, referred to as
183 the *Base* case, uses only the specific humidity tracer in a saturation adjustment scheme modeled
184 after Galewsky et al. (2005) as a direct representation of advection-condensation theory. Any
185 water in excess of saturation (grid-box mean) is assumed to fall out immediately as precipitation.
186 Thus, no clouds are present. The second control simulation is referred to as the *Cloud* case. It

187 carries specific humidity, cloud liquid, cloud ice, and CF tracers through the same large-scale cloud
188 macrophysics scheme as implemented in the GFDL HiRAM model (Zhao et al. 2009). The cloud
189 scheme assumes a beta distribution for sub-grid-scale total water (which includes both WV and
190 CC). CF is diagnosed from this total water-based RH, which varies only slightly from traditional
191 RH (which is based on WV only and is the RH reported in the results). The default beta distribution
192 is such that a grid-mean total water-based RH value exceeding 83.3% (the critical RH: RH_c) allows
193 for sub-grid values greater than 100% and thus a non-zero CF for the grid box.

194 The pathways for conversion between WV, cloud liquid, cloud ice, and hydrometeors follow a
195 Rotstayn-Klein single-moment microphysics scheme (after Rotstayn 1997; Rotstayn et al. 2000).
196 Additionally, as the principal source of WV, surface evaporation is represented by adjusting the
197 specific humidity of grid boxes below ~ 850 hPa towards saturation with an e-folding timescale of
198 30 minutes. Microphysical sources of WV are large-scale (LS) evaporation of cloud liquid, LS
199 sublimation of cloud ice, rain evaporation, and snow sublimation. The only sinks of WV, namely
200 LS condensation and LS deposition, are also the only sources of CC. CC is lost to WV through LS
201 evaporation and LS sublimation, to rain through autoconversion, accretion, and melting of cloud
202 ice, and to snow through gravitational settling. Additionally, cloud liquid is converted to cloud ice
203 through riming, the Bergeron-Findeisen process, and homogeneous freezing, and both cloud ice
204 and snow can be converted to rain through melting. (Cloud ice and snow have identical properties
205 such as fall speed and are simply distinguished by their location in or out of a cloud.) See Fig. 1
206 in Frazer and Ming (2021) and the descriptive text for more details of these conversions.

207 *b. Perturbation Experiments*

208 On the surface, there are three chief distinctions between saturation adjustment (Base control)
209 and a full cloud scheme (Cloud control). First, clouds can form (and thus precipitation is possible)

210 before the grid box is fully saturated through RH_c and an assumed sub-grid-scale RH distribution.
211 Second, the cloud scheme allows precipitation to evaporate before reaching the surface through
212 rain evaporation and snow sublimation (hereafter RESS). Third, cloud condensate may be advected
213 before precipitating out or evaporating. The effects of the first two distinctions can be easily explored
214 by being simply "turned-off" in the cloud scheme. The third is inferred as a residual effect.

215 Each of the three distinctions correspond to the three efficiencies which effect the residence time
216 of water in the atmosphere and form a key part of the analysis. We make use of the explicit/large-
217 scale precipitation efficiency (PE) as defined in Zhao (2014) to represent the total PE, since only
218 stratiform (not convective) precipitation is represented in this model. PE is the ratio of surface
219 precipitation to CC sources (condensation and deposition), and thus represents the fraction of
220 condensed particles which subsequently rain out. Following Langhans et al. (2015), PE can be
221 thought of as the product of a formation efficiency (FE) and a sedimentation efficiency (SE):
222 $PE = FE * SE$. FE represents the probability of formation given condensation, and SE represents
223 the probability of sedimentation given formation. Finally, the condensation efficiency (CE) is
224 the probability of condensation given entrainment into a cloud but is used herein to represent the
225 fraction of atmospheric WV that subsequently condenses. Thus, CE is the ratio of CC sources to
226 WV sources, FE is the ratio of precipitation formation to CC sources, and SE is the ratio of surface
227 precipitation to precipitation formation. Additionally, the residence (or recycling) time for WV in
228 the atmosphere is defined after Trenberth (1998) as the e -folding time constant for the depletion
229 of precipitable water by precipitation, that is, the global ratio of column-integrated WV to the
230 precipitation rate. These indicators of features of the water cycle are used to quantify changes in
231 the WV, CC, and precipitation budgetary terms to supplement the analysis of steady-state fields.
232 But also, as these efficiencies correspond to distinctions between saturation adjustment and a cloud

233 scheme, we intentionally alter the efficiencies to understand the effects on steady-state fields. CE
234 is affected by RH_c , SE is 100% without RESS, and FE cannot be defined without CC.

235 Thus, three principal perturbation experiments are designed, testing sensitivity to condensation,
236 sedimentation, and formation cloud processes. The condensation perturbation focuses on the con-
237 version between WV and CC through cloud macrophysics, specifically sub-grid-scale cloudiness.
238 The first key distinction between saturation adjustment and a cloud scheme can be eliminated
239 by removing sub-grid-scale cloudiness and requiring 100% grid-mean RH for cloud formation.
240 Accordingly, an intermediate setup between the Base and Cloud controls is created by reducing the
241 width parameter of the beta distribution defining sub-grid-scale RH from 0.2 to 0.01, effectively
242 requiring 100% grid-box-mean RH for cloud formation. This perturbation run is referred to as
243 *RHc100* (since effectively $RH_c = 100\%$) with results in Section 3b.

244 The sedimentation perturbation focuses on the role of re-evaporation of hydrometers. While
245 saturation adjustment oversimplifies the variety of conversions in this Rotstayn-Klein microphysics
246 scheme, it is analogous to the LS phase changes and precipitation processes. The chief remaining
247 processes are the recycling of hydrometeors back to WV through RESS. Thus, another intermediate
248 setup between the controls is created to illuminate the significance of RESS. For this experiment—
249 *noRESS* which is presented in Section 3c—the rates of RESS are arbitrarily set to zero. Additionally,
250 to examine the combined effect of the key microphysical and macrophysical differences between
251 the Base and Cloud cases, a final intermediate case is considered. The *RHc100_noRESS* case
252 includes the $RH_c = 100\%$ and omission of RESS effects to examine residual differences between
253 the control cases, which is assumed to correspond to the third key difference between saturation
254 adjustment and full cloud physics—advection of CC—as explored in Section 4.

255 The formation perturbation is not focused directly on a difference between the Base and Cloud
256 cases. In the Base case saturation adjustment, precipitation is formed directly from WV in a manner

257 more similar to condensation than formation. Rather, formation is explored so that sensitivity to
258 all key conversions of the cloud scheme are considered. Formation consists of three major process:
259 autoconversion, accretion, and ice settling. Ice settling is a net term—the difference between ice
260 falling into and out of grid boxes. Accordingly, autoconversion and accretion were isolated as the
261 best processes to perturb in order to explore formation sensitivities. From a general perspective,
262 if autoconversion or accretion is arbitrarily reduced in this model, the other process strengthens to
263 keep formation close to constant, but somewhat reduced. Conversely, if one process is amplified,
264 the other weakens. An analogous effect results from altering the prescribed cloud drop number
265 concentration, N , the default value being 50 m^{-3} , since both autoconversion and accretion are
266 a function of N . For autoconversion to occur, the radius of the cloud droplets—a function of
267 N —must be greater than the critical particle radius threshold at which autoconversion occurs. For
268 accretion, the collection efficiency of a cloud droplet by a liquid droplet is a function of particle
269 size which is a function of N . If N is decreased, autoconversion increases and accretion decreases
270 with a net amplification of formation. An increase of N produces an a opposite effect. Thus,
271 the strength of formation and the balance between autoconversion and accretion have broader
272 significance because of their connection to drop number concentration parameterizations.

273 Here, alterations to autoconversion are used to adjust *accr/auto* (and indirectly explore a key
274 affect of altered N). The principal formation perturbation explored in Section 3d, *halvAUTO*,
275 consists of halving the computed value for autoconversion for each grid box at each time-step. For
276 robustness, a corresponding doubling of of autoconversion, *doubAUTO* is also examined. Note
277 that the halving or doubling of autoconversion is performed in the microphysical code before the
278 enforcement of a limiter which ensures that autoconversion is limited to the amount that reduces
279 local liquid cloud condensate to the critical value at which autoconversion begins (after Rotstayn
280 1997).

281 For all control and perturbation experiments, the atmospheric state of the model (winds, temper-
282 ature, etc.) is identical at every time-step. The various experiments performed are summarized in
283 Table 1. All model runs in this study include a 300-day spin-up of the dry GCM before the next
284 1000 days are averaged. For figures and analysis, data is averaged between the two hemispheres
285 because of the hemispheric symmetry of the simulated climate. 15° to 90° is considered the sub-
286 and extra-tropics (STET) and is the focus of the analysis due to the lack of a convection scheme
287 making the tropics nearly saturated (see Ming and Held 2018).

288 3. Results

289 *a. Controls: Base and Cloud*

290 A budgetary comparison of the control cases is shown in Fig. 1a, which depicts the principal
291 WV tendency terms for the Base and Cloud cases from a column-integrated, zonally-averaged
292 perspective. For the Base case, the WV balance is simply between precipitation from saturation
293 adjustment and surface evaporation. Outside of the tropics (which are not shown), the immediate
294 precipitation dominates in the mid-latitude storm tracks while evaporation occurs mostly in the
295 subtropics, implying significant horizontal advection of water from the subtropics (including
296 that facilitated by mid-latitude baroclinic eddies). For the Cloud case, the dominant balance
297 between net LS condensation (condensation and deposition minus evaporation and sublimation
298 with condensation dominating) as the main WV sink and surface evaporation as the main WV
299 source is similar to the Base case, though RESS does make a non-negligible contribution. Cloud
300 case LS condensation is everywhere stronger than Base case saturation adjustment, while the surface
301 evaporation is nearly indistinguishable except in the high latitudes where Base surface evaporation
302 is negligible. Thus, RESS provides an additional source of WV, strengthening the WV cycle as

303 opposed to replacing surface evaporation as a source. Fig. 1b shows the CC budget applicable
304 only to the Cloud case. Net LS condensation as the source of CC is balanced nearly perfectly
305 latitudinally, implying minimal advection of CC. In the subtropics, autoconversion dominates
306 accretion and ice settling as sinks of CC, but ice settling (snow) dominates poleward of 40° with
307 rain processes becoming negligible poleward of 60°.

308 While precipitation is simply saturation adjustment in the Base case but formation processes
309 minus RESS in the Cloud case, both precipitation and precipitation minus evaporation (P-E) have
310 similar latitudinal distributions in the two cases (Fig. 1c). The principal latitudinal difference is
311 a slight increase in precipitation (and thus P-E) in the extratropics in the Cloud case, where ice
312 settling (a process vastly different than saturation adjustment) dominates as the principal source of
313 precipitation, and surface evaporation decreases in the Base case as discussed previously. Thus,
314 the strength of the hydrological cycle in terms of surface precipitation is largely indistinguishable
315 with a STET average of 1.84 mm/day in the Base case and 1.91 mm/day in the Cloud case (see
316 Table 2 which also shows a similarity in surface evaporation). This correspondence between these
317 idealized saturation adjustment and full cloud microphysics models without any control by radiative
318 balance suggests a significant control of the hydrological cycle by large-scale circulation perhaps
319 mediated through RH (as discussed below).

320 In contrast, the strength of the WV cycle differs greatly between the two control cases. This can
321 be seen in Fig. 2a and b which depict the globally-averaged, column-integrated values and fractions
322 of the sources and sinks in the Base and Cloud cases. The total STET WV sources and sinks in the
323 Cloud case are 3.63×10^{-5} and 2.82×10^{-5} $\text{kg m}^{-2} \text{ s}^{-1}$, respectively, with the regional imbalance
324 implying advection of WV into the tropics (since evaporation is strongest in the subtropics). For
325 comparison, the Base case analogs of surface evaporation (the only WV source) and condensation
326 (the only WV sink) are 2.70×10^{-5} and 2.11×10^{-5} $\text{kg m}^{-2} \text{ s}^{-1}$, respectively. Thus, the strength of

327 the cycling of WV is significantly enhanced in the Cloud model by $\sim 30\%$. Adding more sources
328 and sinks of WV, in particular introducing sources above the boundary layer through RESS, allows
329 for a strengthening of the WV cycle and a slight shortening of the residence time (from 13.1 to
330 12.7 days). In the Cloud case, CC is also cycled where all the WV sinks are CC sources, and
331 precipitation processes are the main CC sinks (see Fig. 2b) with CC sources and sinks balanced in
332 the STET region.

333 This overall picture of water cycling between WV, CC, precipitation, and an assumed surface
334 reservoir can be seen in Fig. 3 and described in terms of efficiencies. For the STET WV produced
335 through surface evaporation, RESS, and evaporation (LS evaporation and sublimation), 83.9%
336 is condensed (through LS condensation and deposition). Of the water condensed, most forms
337 precipitation, while some is evaporated (a very small effect in this model with only a stratiform
338 cloud scheme) resulting in a FE of 98.2% . (Some also persists as condensate but this effect is lost
339 with time-averaging). Of the precipitation formed, $\sim 20\%$ is returned to WV through RESS before
340 reaching the surface resulting in an SE of 79.7% and a PE of 78.3% . These efficiencies, along
341 with precipitation and residence times, are summarized in Table 2. The positive WV reservoir and
342 negative surface reservoir value are again indicative of moisture export (negative P-E) from the
343 STET region.

344 Fig. 3 also shows how a cloud scheme builds on saturation adjustment. In Base case, only two
345 reservoirs—WV and surface—would exist with two arrows between them representing surface
346 evaporation and saturation adjusting. Yet, qualitative similarity exists in the RH distribution of the
347 Base and Cloud cases as shown in Fig. 4a. Both cases have qualitatively realistic free tropospheric
348 RH features: the subtropics and upper troposphere are relatively dry, while the extratropics are
349 moist (Fig. 4a). As noted in Ming and Held (2018), the high RH values in the deep tropics (not
350 shown) and boundary layer (below 850 hPa) are due to the lack of a moist convection scheme and

351 the way in which surface evaporation is modeled, respectively. Fig. 4a suggests that the addition
352 of a cloud scheme has two main effects on the RH distribution, while keeping the main features
353 present. The subtropical dry zones and nearby mid-latitudes are substantially moistened with a
354 peak increase of up to around 5% RH, while much of the polar upper troposphere becomes drier
355 by a similar magnitude. The mechanisms for these changes are investigated in the condensation
356 and sedimentation perturbations. Fig. 4b shows the model isentropes, significant because of the
357 established isentropic transport of moisture from the subtropics as discussed in the introduction.
358 Here, it is clear that the polar upper troposphere (drier in the Cloud case) is connected to the the
359 subtropical boundary layer via isentropes. Yet, the overall similarity between the control cases in
360 the free troposphere implies that RH is controlled to first order by general circulation, as opposed to
361 cloud processes. Thus, in keeping with advection-condensation theory, one does not need detailed
362 cloud information for understanding large-scale (first-order) RH patterns.

363 The cloud fields generated in the Cloud case are shown in Fig. 4c-d. Free tropospheric CF values
364 peak at near 30% in the extratropical storm track region, co-incident with the 75% average RH
365 contour. Liquid cloud condensate (LCC) is concentrated in the boundary layer (unrealistically high
366 because of high RH from artificial surface evaporation as discussed above) with a secondary peak
367 near the storm tracks. Ice cloud condensate is concentrated in a broad region near the storm tracks
368 restricted to freezing temperatures (see Fig. 4b). LCC, with its higher magnitude, dominates the
369 spatial pattern of total CC), which is the sum of ice and liquid water mixing ratios. Since the focus
370 of this study is on total clouds, not on the distribution of ice versus liquid, the remainder of this
371 work will consider only total CC, which is concentrated in the tropics with a secondary peak in the
372 storm tracks.

373 *b. Condensation Perturbations: RHc100*

374 As discussed in the introduction, since isentropic transport is the key source of WV for the polar
375 regions, cloud formation (and precipitation) in the extratropical storm tracks provides a limiting
376 effect on the amount of WV reaching the polar regions. In the Cloud case, cloud formation
377 (required for precipitation) takes place when grid-mean RH (as defined by total water) exceeds
378 83.3%. Therefore one might expect a correlation between the model's extratropical cloud maxima
379 (storm tracks) in the model and 83.3% RH contours. But cloud formation is based on instantaneous
380 RH, not the long-term averages shown in Fig. 4c where the storm tracks are roughly co-located
381 with the 75% RH contours. Higher RH values may occur equatorward of a given RH contour.
382 Allowing for time variability in RH renews the possibility of a connection between the location of
383 the storm tracks and RH distribution because of RH_c . This possible connection is explored with
384 the RHc100 run, where the cloud scheme is adjusted to require essentially 100% grid-mean RH
385 for cloud formation.

386 In the RHc100 case, the entire WV/CC cycle slows down significantly compared to the Cloud
387 case (see Fig. 2b and c). Since clouds are now unlikely to form and remove moisture from the
388 atmosphere below 850 hPa (where the air is generally nearly, but not quite, saturated), surface
389 evaporation decreases (Fig. 5a). RESS play less of a role as WV sources, approximately half of
390 both the magnitude and percentage as in the Cloud case, and become nearly non-existent in the
391 extratropics. LS condensation decreases as a WV sink and CC source; the slowdown increases the
392 WV residence time by 2.6 days or 13% (Table 2).

393 CE decreases only slightly (3%) despite the intense perturbation in condensation. CE is not a
394 measure of how fast WV condenses, but simply whether it eventually does (in the given region
395 which here is the STET region). Similarly, FE decreases by 3% with a greater weakening of

396 formation processes than condensation (see Fig. 5b). FE represents the likelihood that a water
397 molecule, once it condenses, forms precipitation. Here, FE decreases since LS evaporation and
398 sublimation have increased both in value and as a percentage of LS condensation/deposition. In the
399 RHc100 setup, once a cloud is formed, if it persists to another time-step where RH has decreased
400 (as from precipitation), the remaining cloud condensate must entirely re-evaporate/sublimate. In
401 contrast, in the Cloud case, only enough cloud condensate to match the RH-based PDF must
402 evaporate, as long as grid-box-mean RH is above 83.3%.

403 The most significant change in efficiencies is SE which increases from 79.7% to 89.4% resulting
404 in an amplification in PE ($= FE * SE$) from 78.3% to 85.1%. SE increases because of the drastic
405 decrease in RESS from both decreased precipitation formation (Fig. 5c) as well as increased steady-
406 state RH (Fig. 5d). RH is significantly increased in regions where cloud formation at less than 100%
407 RH had kept WV from being transported. Thus, more WV is isentropically transported to the polar
408 upper troposphere before clouds are formed. Weakened RESS results from less precipitation falling
409 through moister air, especially in the extratropics where the increase in RH is most significant.
410 Ultimately, despite increased PE, there is a 10% reduction in STET surface precipitation (Table 2)
411 potentially driven by decreased CC in the boundary layer (discussed below).

412 In addition to an increase in RH, with the RHc100 setup, CF is significantly amplified in the
413 polar extratropics (Fig. 5e). With seemingly more difficult conditions for cloud formation, CF
414 increases everywhere (above 850 hPa). This can be understood by considering what triggers cloud
415 formation in the cloud scheme: high values of RH. The increase in average RH noted previously
416 does in fact correspond to a rise in occurrences of high RH as shown through a histogram of daily
417 RH values (Fig. 5g) where values in the [100%, 105%] bin increase drastically, but all other values
418 decrease slightly. A histogram of daily CF values (Fig. 5h) shows a decrease in CF values below
419 65% and a drastic rise in occurrences of the highest values with the final bin being the highest

420 populated. (Note that while RH values greater than 100% are possible, by definition, 100% is the
421 maximum possible CF value such that the final CF histogram bin represents values of exactly 100%
422 CF.) With 100% grid-mean RH required for cloud formation, when cloud formation is triggered it
423 must be 100% CF at the time-step of the model. These histograms were further broken down by
424 meridional and vertical flow direction (not shown). Poleward and upward flows accounted for the
425 highest RH values and thus the higher CF values, but overall the stratified histograms painted the
426 same picture. For every direction of flow, the RHc100 perturbation requires greater RH for cloud
427 formation, increasing high RH values and thus CF. Accordingly, the location of maximum storm
428 track cloudiness shifts poleward (to areas of greater RH) from $\sim 50^\circ$ (Fig. 4c) to $\sim 60^\circ$ (not shown).

429 While CF increases significantly, the change in CC in the free troposphere is small, and in most
430 places is a decrease as seen in Fig. 5f. (A significant loss of CC below 850 hPa not shown is a
431 result of the region being generally unsaturated, since surface evaporation is associated with a time
432 scale.) While changes in CF and CC need not totally align, such drastic differences are surprising
433 and are, in fact, largely an artifact of altering the macrophysics in a way that is unexpected by
434 the microphysics scheme. With the RHc100 condition, if clouds form in a grid cell, the grid cell
435 CF is 100%. Yet with higher CF, autoconversion decreases. In the microphysics scheme, the rate
436 of change of cloud liquid due to autoconversion is proportional to $CF * (LCC/CF)^{(7/3)}$ or, in a
437 frequently-invoked limiter, $\ln(LCC/CF) * LCC$ (see Rotstayn 1997). In other words, if CC is more
438 widely distributed over a higher CF, it triggers less autoconversion. So a rise in CF, unmatched by
439 an increase in CC (since CC is in fact more difficult to form with the RHc100 condition), causes a
440 decrease in autoconversion leading to a cycle slowdown as expected. This result highlights both
441 the non-interchangeability of CC and CF as cloud tracers and the importance of considering the
442 details of a microphysics scheme when evaluating the usefulness of performing drastic alterations.

443 The bigger picture highlighted by the RHc100 case is the significance of isentropic flow and
444 the way in which details of the macrophysics scheme can thus have such significant effects.
445 (Accounting for such phenomena is lacking in advection-condensation theory.) Here, sub-grid-
446 scale RH has a significant effect on extratropical clouds by affecting the storm track locations and
447 altering the frequency of high-RH values. Re-located storm tracks could also have significant
448 effects on shortwave radiation not explored here, contributing to the usefulness of RH_c as a tuning
449 parameter for radiative balance. A potential emergent constraint on storm track response (which
450 varies significantly in GCMs as noted in Bender et al. 2011) could inform RH_c choice. Thus,
451 the RHc100 case also emphasizes the additional, non-radiative, impacts of tuning through RH_c ,
452 particularly on redistributing WV and precipitation.

453 *c. Sedimentation Perturbations: noRESS*

454 As described previously, one of the most noteworthy differences between saturation adjustment
455 and a full cloud scheme is the addition of two significant sources of WV: RESS. As seen in Fig. 1,
456 column-integrated RESS have a significant presence at all latitudes, providing an even stronger
457 source of WV than surface evaporation poleward of approximately 50° . Fig. 2b shows that together
458 they contribute approximately 17% to STET WV sources. RESS defines SE as shown in Fig. 3
459 with one-fifth of formed precipitation lost to RESS. Fig. 6a depicts the changes in WV tendencies
460 when RESS is no longer present in the Cloud scheme. While surface evaporation increases, the
461 elimination of RESS yields a net decrease in WV sources (Fig. 2d). Matching this decrease,
462 a reduction in LS condensation/deposition (WV sinks) is spatially correlated both latitudinally
463 and vertically with the eliminated RESS. Thus, as in the RHc100 case, WV and CC cycling is
464 weakened: the total WV/CC sources or sinks in noRESS are 13-16% less than in the Cloud case,
465 while still greater than in the Base case (see Fig. 2). However, at the same time, the residence time

466 of a water molecule in the atmosphere is decreased by 7% due to the elimination of RESS as WV
467 sources which come from recycled hydrometeors.

468 Without RESS as sinks of precipitation, STET precipitation increases by $\sim 5\%$ (8% globally)
469 as seen in Fig. 6c and Table 2. By definition, without RESS, SE is 100%. As FE is nearly
470 unchanged, PE increases drastically from 78.3% to 97.9% with a moderate increase in precipitation.
471 The elimination of snow sublimation corresponds strongly with the pattern and magnitude of a
472 decrease in ice settling yielding only a slight change in precipitation poleward of 45° . However, in
473 the subtropics, the elimination of rain evaporation is unmatched by decreases in autoconversion and
474 accretion, so the precipitation increase is mostly subtropical, while the storm tracks are virtually
475 unaffected.

476 This feature can be rationalized by considering the location of WV sources and sinks and
477 the connection between these budgetary terms and the steady-state fields. From a steady-state
478 perspective, the role of RESS in redistributing WV and moistening the atmosphere can be seen
479 in Fig. 6d. Turning off RESS results in a significant decrease in RH (up to 6%), especially in the
480 subtropics and the polar lower troposphere. Additional experiments were performed with RESS
481 turned off locally, including only between 15° and 45° or elsewhere (not shown). These runs
482 resulted in RH being only reduced (with any significance) in the regions where RESS is turned
483 off, demonstrating the local nature of the contribution of RESS to moisture. In redistributing
484 WV, RESS also plays a significant role in the cloud distribution. Without RESS, both CF and CC
485 decrease globally as shown in Fig. 6e-f. The change in CF is of a similar pattern to the change in RH
486 in the polar extratropics, while the change in CC is more concentrated in the storm tracks (where CC
487 is larger to begin with). RH and CF changes are directly connected, as confirmed by considering
488 histograms of extratropical RH and CF (Fig. 6g-h). The noRESS case shifts occurrences of

489 RH away from higher values ($>95\%$) in the extratropical free troposphere corresponding with a
490 decrease in CF concentrated where RH values are highest to begin with.

491 The connection between budgetary and steady-state changes is nuanced. Globally, the general
492 reduction in RH is to be expected since the lack of RESS results in a drying of the boundary
493 layer. This drying triggers more surface evaporation, but no others sources of WV. Decreased
494 higher values of RH leads to decreased clouds. But, spatially, the areas of largest RH change
495 (free troposphere, especially the polar extratropics) do not coincide with the locations of largest
496 RESS tendency. RESS provides a significant source of WV throughout the boundary layer and
497 free troposphere, especially in the tropics (not shown). However, while RESS is smallest in the
498 extratropics, its relative importance as a source of WV is greatest there (see Fig. 1a). While surface
499 evaporation can easily increase below 850 hPa to replace RESS as a source of WV in the boundary
500 layer (which is always nearly saturated), its ability to replenish moisture above 850 hPa depends
501 on circulation. The rising motions induced by the Hadley circulation in the tropics allow humidity
502 (and thus clouds) to be less affected by the loss of RESS. In contrast, in the polar regions where
503 less vertical motion takes place and horizontal transport is more important for WV, the lower
504 troposphere above 850 hPa experiences significant drying. From an isentropic perspective, the
505 drier extratropics can be thought of as the result of less moisture being supplied to the mid-latitude
506 eddies so that less WV is condensed near the poles. The decrease in LS condensation is consistent
507 with a smaller isentropic WV gradient.

508 Thus, in the storm tracks and high latitudes, the increase in precipitation is small since the
509 elimination of RESS dries the region creating two opposing effects. Precipitation is increased
510 since SE is now 100%, but this increase is nearly balanced by a reduction in precipitation due to
511 less moisture and thus fewer precipitating clouds in the region. However, in the subtropics and mid
512 latitudes, the direct increase in precipitation is largely unbalanced since clouds are less affected

513 (as clouds are few to begin with so humidity decreases have little effect). This local role of RESS
514 is further seen in the fact that P-E (Fig. 6c) remains largely unchanged. Ultimately, the role of
515 RESS in the free troposphere is to increase RH (and ultimately clouds) by providing an additional
516 source of WV, while decreasing precipitation and—to a much greater extent—the PE through the
517 introduction of an atmospheric sink for hydrometeors.

518 *d. Formation Perturbation: halvAUTO*

519 In the halvAUTO case, autoconversion decreases in the STET region by 29%. Accretion and ice
520 settling increase by 19% and 4%, respectively, to keep total STET CC sinks only 3% less than in
521 the Cloud case. This re-balancing can be conceptualized as weakened autoconversion causing
522 more cloud liquid to be present to be scavenged by ice through accretion and subsequently settling.
523 Similarly, in the doubAUTO case, STET autoconversion increases by 34%, accretion decreases
524 by 22%, and ice settling increases by 6%, such that total CC sinks are only 3% more than in the
525 Cloud case. These changes can be seen in Fig. 2e and f. In both cases the relative balances of the
526 WV sources and sinks is roughly unchanged with a slight re-balancing of RESS as snow increases
527 with a decrease of rain in halvAUTO and vice versa in doubAUTO. Noting the parallel opposing
528 changes in halvAUTO and doubAUTO, we focus primarily on halvAUTO.

529 Fig. 7a shows that latitudinally the WV balance is unchanged with decreases in LS condensation,
530 surface evaporation, and rain evaporation balancing each other. Similarly, the CC balance (Fig. 7b)
531 stays latitudinally unchanged with a decrease in LS condensation balanced by the net decreases
532 in CC sinks. The opposing changes in autoconversion and accretion are similar in their spatial
533 pattern, but the decrease in autoconversion is stronger, resulting in less precipitation as shown in
534 Fig. 7c. These changes are principally equatorward of 60° since that is where autoconversion is
535 most significant in the first place (Fig. 1b).

536 Across the STET region, precipitation decreases in the halvAUTO case by 3% and increases in
537 the doubAUTO case by 4%, similar to how the strength of the WV/CC cycle changes. From an
538 efficiency perspective (see Table 2), CE and FE change slightly in the same direction as changes
539 in precipitation, decreasing in halvAUTO in line with a cycle slowdown. SE also changes slightly
540 but in the opposite way: with decreased net formation but a proportionally larger decrease in
541 RESS in the halvAUTO case, SE increases slightly. The FE and SE effects balance such that PE
542 is minimally affected. This finding holds true for smaller and larger alterations to autoconversion,
543 accretion, and N except when an artificial decrease in a process is so large that the other processes
544 cannot keep the WV/CC cycle roughly constant. For example, when autoconversion is completely
545 eliminated, total STET CC sinks decrease by 6% as accretion cannot come close to making up for
546 the difference reducing FE to 90.4% and PE to 72.1%. However, apart from such limiting cases,
547 changes in budgetary terms and efficiencies are roughly linear. The residence time increases with
548 halvAUTO with weakened precipitation since a water molecule now spends a longer time in the
549 atmosphere as CC before precipitating, while the doubAUTO case shows a corresponding decrease
550 in residence time.

551 From a steady-state perspective, in the halvAUTO case, RH, CF, and CC all increase as shown in
552 Fig. 7d-f. The significant changes are spatially similar, concentrated equatorward of 60° (where the
553 net decrease in CC sinks was strongest) and below ~ 500 hPa, peaking in the storm tracks. These
554 steady-state changes described are qualitatively opposite in the doubAUTO case (not shown). Of
555 note, the steady-state RH and cloud fields change not in response to a shift in the balance between
556 autoconversion and accretion, but in response to changes in total sources/sinks. When WV/CC
557 cycling strengthened due to increased autoconversion, increased accretion, or decreased N , an
558 amplification of RH, CF, and CC resulted. Opposite changes are associated with WV/CC cycling

559 weakening. Re-balancing autoconversion and accretion must have a relatively innocuous effect on
560 RH and clouds in and of itself.

561 Why does a strengthened (weakened) cycle increase (decrease) RH and clouds? It is important
562 to note that this generalization does not extend past these perturbations. (The pattern is followed
563 in the RHc100 case discussed previously but not in the noRESS case, possibly because of the
564 significant spatial and physical differences resulting from replacing RESS as WV sources with
565 enhanced surface evaporation.) However, in the absence of other changes (such as adding sources
566 and sinks from the Base to the Cloud case), a longer (shorter) residence time for a water molecule
567 in the atmosphere could be expected to correspond to an increase (decrease) in the steady-state
568 fields which represent the forms that a water molecule takes as it resides in the atmosphere.
569 Additionally, steady-state RH is directly connected to the WV cycle through surface evaporation
570 since it is formulated as a function of subsaturation. RH is connected to CF as demonstrated by
571 considering histograms of RH and CF (Fig. 7): the halvAUTO case slightly shifts occurrences
572 of RH toward the highest values (>100%). Without any significant changes to the cloud physics
573 beyond a re-balancing of autoconversion and accretion, CC can logically be expected to follow CF.
574 Thus, the formation perturbations demonstrate the resilience of this cloud microphysics scheme
575 to changes in the balance of formation tendencies in terms of PE. Additionally, the general patterns
576 for steady-state consequences of the WV/CC cycle weakening (strengthening) emerge showing how
577 steady-state fields are affected by changes in residence time. A weakened (strengthened) cycle,
578 apart from other changes in cloud physics, leads to an increased (decreased) residence time and
579 diminished (amplified) steady-state RH, CC, and CF.

580 **4. Discussion and Conclusions**

581 *a. Summary*

582 The general picture that emerges from this idealized modeling study is that circulation sets the
583 basic pattern of moisture and precipitation, as seen through the first order similarity between the two
584 control cases. In the perturbation runs, details of the physics of condensation and sedimentation
585 also have substantial effects on humidity, clouds, and precipitation. However, it is noteworthy
586 that while RH does differ substantially (in certain extratropical regions) between the control
587 cases, precipitation does not, as the precipitation changes in the condensation and sedimentation
588 perturbations (RHc100 and noRESS) are of opposing sign. A secondary picture is the utility of
589 this idealized GCM for understanding physical controls of free tropospheric clouds and responses
590 to perturbations since key processes can be cleanly isolated. The saturation adjustment scheme
591 (Base case) shows gross RH features, as expected from advection-condensation theory, but cloud
592 processes refine the features. In particular, cloud macrophysics are important since thresholds
593 for cloud formation change cloud distribution (including the CF/CC ratio) and hence RH due to
594 isentropic transport of moisture as shown in the RHc100 run. Cloud microphysics are equally
595 important, adding a key component through the re-evaporation of hydrometeors (RESS) changing
596 RH values by a similar magnitude, as much as 5-6%. However, the formation perturbations
597 demonstrate that the balance of precipitation-forming processes (here autoconversion and accretion)
598 have little significance for RH, cloudiness, precipitation, and especially PE.

599 *b. Advection-Condensation Theory*

600 As was discussed previously, there are, on the surface, three differences between a saturation
601 adjustment scheme (or advection-condensation theory) and a full cloud scheme: RH_c , RESS, and

602 presence of CC which can be advected and/or subject to LS evaporation/sublimation. The first
603 two differences are here individually directly removed, but the third must be explored as a residual
604 in the *RHc100_noRESS* experiment where we remove the RH_c and RESS effects together from
605 the Cloud case. If these three identified differences are exhaustive, *RHc100_noRESS* represents
606 the effect of adding CC to the Base case. Additionally, if the RH_c and RESS effects are linearly
607 additive, we can mathematically manipulate the various experiments to isolate the separate effects
608 of RH_c and RESS added to the Base case (as opposed to removing these effects from the Cloud case
609 as was described in the Results section). To this end, Fig. 8 explores to what extent the RH_c and
610 RESS effects are linearly additive, to what extent they can explain the full difference between the
611 Base and Cloud controls, and the characteristics of the residual differences which can be attributed
612 to CC advection.

613 The *RHc100* run includes RESS and advection effects, the *noRESS* run includes RH_c and
614 advection effects, and the *RHc100_noRESS* run is just the advection effect. So we can test for
615 linearity of the RH_c and RESS effects by comparing *RHc100* plus *noRESS* minus *RHc100_noRESS*
616 (Fig. 8a). The combination appears to be mostly linear except in the free tropospheric high latitudes
617 where both *RHc100* and *noRESS* runs had significant, but opposing, effects. *RHc100* leads to
618 moistening and *noRESS* to drying; linear addition over-emphasizes drying or under-emphasizes
619 moistening. A possible mechanism is that when both are implemented, there is less moisture (from
620 *noRESS*) to be exported to the high latitudes (in *RHc100*), but this effect should be minimal as
621 *noRESS* minimally dries the boundary layer. A more like explanation is that since in *RHc100*,
622 RESS decreases by over 50%, the *noRESS* drying effect is dampened when combined. But since
623 they combine nearly linearly, we can separately analyze the three effects of adding a cloud scheme
624 to a saturation adjustment scheme.

625 When adding a cloud scheme to a saturation adjustment scheme, advection and LS evapora-
626 tion/sublimation (and any other residual effects, for example, nucleation barrier and incomplete
627 fallout in cirrus as noted by Liu et al. (2010)) moistens the free tropospheric subtropics and mid-
628 latitudes (Fig. 8b) as well as the polar stratosphere. Implementing a RH_c of 83.3% dries the high
629 latitudes (Fig. 8c) by allowing for more condensation and precipitation of moisture before it is
630 isentropically transported to the poles. Finally RESS moistens the free troposphere, most strongly
631 in the storm tracks and lower polar regions (Fig. 8d), by adding an additional source of WV above
632 the boundary layer.

633 Thus, this work highlights the key deficiencies with an advection-condensation paradigm. The
634 relatively small residual effects seen when comparing RH_{c100_noRESS} minus Base to Cloud
635 minus base (Fig. 8b) suggest that RH_c and RESS are the key ways in which a cloud scheme alters
636 the RH distribution from advection-condensation theory alone, in the absence of cloud processes
637 altering the circulation through latent heat release or cloud radiative effects. RESS is a cloud micro-
638 physical effect already noted as missing from the advection-condensation paradigm and important
639 to moistening the subtropics. But here we also highlight its important for moistening the polar
640 regions where less vertical motion makes surface evaporation less effective at moistening the free
641 troposphere. In contrast, RH_c is a macrophysical effect, an artifact of parameterizations attempting
642 to represent the RH variability present in the real world. Here we emphasize the importance of
643 considering sub-grid-scale humidity distribution to allow clouds to form in appropriate latitudinal
644 locations (a problem that increased resolution alone may not fix). As Sherwood et al. (2010) noted,
645 these components of why the advection-condensation is inadequate are critical to understand in
646 order to accurately model not just climatological values, but importantly changes in RH (and hence
647 clouds and precipitation) with warming.

648 *c. Outlook*

649 The picture presented here is likely to change significantly with warming. While the advection-
650 condensation paradigm suggests that free tropospheric RH is unlikely to change significantly with
651 uniform warming (Sherwood et al. 2010), the specific deficiencies of advection-condensation
652 theory explored here confound predicting changes in RH with warming, already complicated by
653 non-uniform warming. Any changes in RH could also have implications for P-E changes, as the
654 wet-get-wetter paradigm (Held and Soden 2006) is predicated on unchanged lower-tropospheric RH
655 and flow. Sherwood et al. (2014) identified a mixing-induced low cloud feedback where enhanced
656 mixing with warming dehydrates the boundary layer. Here, as in advection-condensation theory,
657 we highlighted the connection between subtropical boundary layer humidity and polar upper
658 tropospheric humidity because of eddy isentropic transport. In addition to the complications of
659 dynamical effects, because of the Clausius-Clapeyron relation, WV transport is expected to increase
660 with warming for thermodynamic reasons (Lavers et al. 2015). And as noted in the introduction,
661 replacement of ice with liquid in mixed-phase clouds with warming may also effect moisture and
662 cloud distribution through changes in precipitation efficiency. Thus, modeling the mechanisms
663 controlling extratropical humidity and clouds accurately is critical for confidently forecasting future
664 change.

665 Our perturbation results demonstrate the significance of key processes for defining steady-state
666 patterns of humidity and cloudiness, implying a strong need to constrain processes such as RESS and
667 sub-grid-scale RH in order to ensure the physical grounding of parameterizations so that responses
668 to altered forcings will also be physical. Additionally, while *accr/auto* (or *N*) was not important
669 here in terms of affecting steady-state fields or average precipitation, it is likely to have other effects
670 as discussed in the introduction, including modulating the intensity of precipitation events. Our

671 results suggest that the strength of warm rain processes as a whole (accretion+autoconversion) plays
672 a role in defining RH, clouds, and precipitation distribution and thus is an important parameter
673 to constrain, not just *accr/auto*. By separately analyzing the effects on CF and CC and their
674 connection to changes in RH and various components of the water cycle, this study highlighted the
675 need to carefully dissect the physical mechanisms for change instead of relying on generalizations.
676 For example, as demonstrated in the RHc100 perturbation, cloud response cannot be directly
677 predicted from changes in average RH. Relationships among RH, CF, and CC in a cloud scheme
678 may be nonintuitive and are certainly nontrivial.

679 Comparing the significance of various controls of clouds cannot be precise in this idealized,
680 decoupled framework. Nor does this study explore the relative significance of various cloud
681 feedbacks to anthropogenic forcings. Yet, by allowing for a detailed exploration of cloud physics
682 decoupled from circulation, this type of idealized model could play a key role in the model
683 hierarchy for reducing uncertainty surrounding cloud feedback. In comprehensive GCMs with
684 coupled feedbacks, circulation feedbacks (particularly shifts in the extratropical jets) have been
685 demonstrated to be less significant than thermodynamic mechanisms of mixed-phase clouds in
686 creating the shortwave extratropical cloud feedback (Wall and Hartmann 2015; Ceppi and Hartmann
687 2016). This finding suggests that cloud parameterization mechanisms relating to mixed-phase
688 clouds may play a significant role in constraining extratropical cloudiness, an area explored in
689 related work with the idealized setup used in this paper (Frazer and Ming 2021).

690 In summary, this study takes a step forward in elucidating physical mechanisms controlling
691 extratropical clouds, while highlighting the importance of identifying and adequately representing
692 these mechanisms in order to accurately simulate the cloud feedbacks associated with climate
693 change.

694 *Acknowledgments.* The authors acknowledge Nadir Jeevanjee, David Paynter, and Daniel Mc-
695 Coy for helpful feedback. M.E.F. was supported by award NA18OAR4320123 from the Na-
696 tional Oceanic and Atmospheric Administration, U.S. Department of Commerce, and award
697 AWD1005319 from the National Science Foundation.

698 *Data availability statement.* The output from the simulations described in this manuscript is
699 archived at the Geophysical Fluid Dynamics Laboratory and is available upon request.

700 **References**

701 Bender, F. A. M., V. Ramanathan, and G. Tselioudis, 2011: Changes in extratropical storm track
702 cloudiness 1983–2008: observational support for a poleward shift. *Climate Dyn.*, **38**, 2037–2053,
703 doi:10.1007/s00382-011-1065-6.

704 Bony, S., and Coauthors, 2015: Clouds, circulation and climate sensitivity. *Nat. Geosci.*, **8**, 261–
705 268, doi:10.1038/ngeo2398.

706 Ceppi, P., F. Briant, M. D. Zelinka, and D. L. Hartmann, 2017: Cloud feedback mechanisms and
707 their representation in global climate models. *WIREs Clim. Change*, **8**, doi:10.1002/wcc.465.

708 Ceppi, P., and D. L. Hartmann, 2016: Clouds and the atmospheric circulation response to warming.
709 *J. Climate*, **29**, 783–799, doi:10.1175/JCLI-D-15-0394.1.

710 Ceppi, P., D. L. Hartmann, and M. J. Webb, 2016: Mechanisms of the negative shortwave cloud
711 feedback in middle to high latitudes. *J. Climate*, **29**, 139–157, doi:10.1175/JCLI-D-15-0327.1.

712 Frazer, M. E., and Y. Ming, 2021: Understanding the extratropical liquid water path feedback in
713 mixed-phase clouds with an idealized global climate model. *Under revision in J. Climate*.

- 714 Frierson, D. M. W., I. M. Held, and P. Zurita-Gotor, 2006: A gray-radiation aquaplanet moist GCM.
715 Part I: Static stability and eddy scale. *J. Atmos. Sci.*, **63**, 2548–2566, doi:10.1175/JAS3753.1.
- 716 Galewsky, J., A. Sobel, and I. M. Held, 2005: Diagnosis of subtropical humidity dynamics using
717 tracers of last saturation. *J. Atmos. Sci.*, **62**, 3353–3367, doi:10.1175/JAS3533.1.
- 718 Geoffroy, O., S. C. Sherwood, and D. Fuchs, 2017: On the role of the stratiform cloud scheme
719 in the inter-model spread of cloud feedback. *J. Adv. Model. Earth Syst.*, **9**, 423–437, doi:
720 10.1002/2016MS000846.
- 721 Gettelman, A., H. Morrison, C. R. Terai, and R. Wood, 2013: Microphysical process rates
722 and global aerosol-cloud interactions. *Atmos. Chem. Phys.*, **13**, 9855–9867, doi:10.5194/
723 acp-13-9855-2013.
- 724 Gettelman, A., H. Morrison, C. R. Terai, and R. Wood, 2014: Corrigendum to "Microphysical
725 process rates and global aerosol-cloud interactions". *Atmos. Chem. Phys.*, **14**, 9099–9103, doi:
726 10.5194/acp-14-9099-2014.
- 727 Held, I. M., 2005: The gap between simulation and understanding in climate modeling. *Bull. Amer.*
728 *Meteor. Soc.*, **86**, 1609–1614, doi:10.1175/BAMS-86-11-1609.
- 729 Held, I. M., 2014: Simplicity amid complexity. *Science*, **343**, 1206–1207, doi:10.1126/science.
730 1248447.
- 731 Held, I. M., and T. Schneider, 1999: The surface branch of the zonally averaged mass transport
732 circulation in the troposphere. *J. Atmos. Sci.*, **56**, 1688–1697, doi:10.1175/1520-0469(1999)
733 056<1688:TSBOTZ>2.0.CO;2.
- 734 Held, I. M., and B. J. Soden, 2006: Robust responses of the hydrological cycle to global warming.
735 *J. Climate*, **19**, 5686–5699, doi:10.1175/JCLI3990.1.

- 736 Held, I. M., and M. J. Suarez, 1994: A proposal for the intercomparison of the dynamical
737 cores of atmospheric general circulation models. *Bull. Amer. Meteor. Soc.*, **75**, 1825–1830,
738 doi:10.1175/1520-0477(1994)075<1825:APFTIO>2.0.CO;2.
- 739 Jeevanjee, N., P. Hassanzadeh, S. Hill, and A. Sheshadri, 2017: A perspective on climate model
740 hierarchies. *J. Adv. Model. Earth Syst.*, **9**, 1760–1771, doi:10.1002/2017MS001038.
- 741 Jiang, H., G. Feingold, and A. Sorooshian, 2010: Effect of aerosol on the susceptibility and
742 efficiency of precipitation in warm trade cumulus clouds. *J. Atmos. Sci.*, **67**, 3525–3540, doi:
743 10.1175/2010JAS3484.1.
- 744 Jing, X., K. Suzuki, H. Guo, D. Goto, T. Ogura, T. Koshiro, and J. Mülmenstädt, 2017: A multi-
745 model study on warm precipitation biases in global models compared to satellite observations.
746 *J. Geophys. Res. Atmos.*, **122**, 11 806–11 824, doi:10.1002/2017JD027310.
- 747 Kelly, K., A. Tuck, and T. Davies, 1991: Wintertime asymmetry of upper tropospheric water
748 between the Northern and Southern Hemispheres. *Nature*, **353**, 244–247, doi:10.1038/353244a0.
- 749 Klein, S. A., and Coauthors, 2009: Intercomparison of model simulations of mixed-phase clouds
750 observed during the ARM Mixed-Phase Arctic Cloud Experiment. I: Single-layer cloud. *Quart.*
751 *J. Roy. Meteor. Soc.*, **135**, 979–1002, doi:10.1002/qj.416.
- 752 Laliberté, F., T. Shaw, and O. Pauluis, 2012: Moist recirculation and water vapor transport on dry
753 isentropes. *J. Atmos. Sci.*, **69**, 875–890, doi:10.1175/JAS-D-11-0124.1.
- 754 Langhans, W., K. Yeo, and D. M. Romps, 2015: Lagrangian investigation of the precipitation
755 efficiency of convective clouds. *J. Atmos. Sci.*, **72**, 1045–1062, doi:10.1175/JAS-D-14-0159.1.

- 756 Lavers, D. A., F. M. Ralph, D. E. Waliser, A. Gershunov, and M. D. Dettinger, 2015: Climate
757 change intensification of horizontal water vapor transport in CMIP5. *Geophys. Res. Lett.*, **42**,
758 5617–5625, doi:10.1002/2015GL064672.
- 759 Liu, Y. S., S. Fueglistaler, and P. H. Haynes, 2010: Advection-condensation paradigm for strato-
760 spheric water vapor. *J. Geophys. Res. Atmos.*, **115**, D24 307, doi:10.1029/2010JD014352.
- 761 McCoy, D. T., D. L. Hartmann, and M. D. Zelinka, 2018: Mixed-phase cloud feedbacks. *Mixed-
762 Phase Clouds: Observations and Modeling*, C. Andronache, Ed., Elsevier, 215–236, doi:10.
763 1016/B978-0-12-810549-8.00009-X.
- 764 McCoy, D. T., D. L. Hartmann, M. D. Zelinka, P. Ceppi, and D. P. Grosvenor, 2015: Mixed-phase
765 cloud physics and Southern Ocean cloud feedback in climate models. *J. Geophys. Res. Atmos.*,
766 **120**, 9539–9554, doi:10.1002/2015JD023603.
- 767 McCoy, D. T., I. Tan, D. L. Hartmann, M. D. Zelinka, and T. Storelvmo, 2016: On the relationships
768 among cloud cover, mixed-phase partitioning, and planetary albedo in GCMs. *J. Adv. Model.
769 Earth Syst.*, **8**, 650–668, doi:10.1002/2015MS000589.
- 770 Michibata, T., and T. Takemura, 2015: Evaluation of autoconversion schemes in a single model
771 framework with satellite observations. *J. Geophys. Res. Atmos.*, **120**, 9570–9590, doi:10.1002/
772 2015JD023818.
- 773 Ming, Y., and I. M. Held, 2018: Modeling water vapor and clouds as passive tracers in an idealized
774 GCM. *J. Climate*, **31**, 775–786, doi:10.1175/JCLI-D-16-0812.1.
- 775 Pierrehumbert, R. T., 1998: Lateral mixing as a source of subtropical water vapor. *Geophys. Res.
776 Lett.*, **25**, 151–154, doi:10.1029/97GL03563.

777 Pierrehumbert, R. T., H. Brogniez, and R. Roca, 2007: On the relative humidity of the atmosphere.
778 *The Global Circulation of the Atmosphere*, T. Schneider, and A. H. Sobel, Eds., Princeton
779 University Press, 143–185.

780 Quaas, J., and Coauthors, 2020: Constraining the Twomey effect from satellite observations: issues
781 and perspectives. *Atmos. Chem. Phys.*, **20**, 15 079–15 099, doi:10.5194/acp-20-15079-2020.

782 Rotstayn, L. D., 1997: A physically based scheme for the treatment of stratiform clouds and
783 precipitation in large-scale models. I: Description and evaluation of the microphysical processes.
784 *Q. J. R. Meteorol. Soc.*, **123**, 1227–1282.

785 Rotstayn, L. D., B. F. Ryan, and J. J. Katzfey, 2000: A scheme for calculation of the liquid fraction
786 in mixed-phase clouds in large-scale models. *Mon. Wea. Rev.*, **128**, 1070–1088.

787 Shepherd, T. G., 2014: Atmospheric circulation as a source of uncertainty in climate change
788 projections. *Nat. Geosci.*, **7**, 703–708, doi:10.1038/ngeo2253.

789 Sherwood, S., S. Bony, and J.-L. Dufresne, 2014: Spread in model climate sensitivity traced to
790 atmospheric convective mixing. *Nature*, **505**, 37–42, doi:10.1038/nature12829.

791 Sherwood, S. C., R. Roca, T. M. Weckwerth, and N. G. Andronova, 2010: Tropospheric water
792 vapor, convection, and climate. *Rev. Geophys.*, **48**, doi:10.1029/2009RG000301.

793 Sherwood, S. C., and Coauthors, 2020: An assessment of Earth’s climate sensitivity using multiple
794 lines of evidence. *Reviews of Geophysics*, **58**, e2019RG000678, doi:10.1029/2019RG000678.

795 Stephens, G. L., 1978: Radiation profiles in extended water clouds. II. Parameterization schemes.
796 *J. Atmos. Sci.*, **35**, 2123–2132, doi:10.1175/1520-0469(1978)035<2123:RPIEWC>2.0.CO;2.

797 Stevens, B., and S. Bony, 2013: What are climate models missing? *Science*, **340**, 1053–1054,
798 doi:10.1126/science.1237554.

- 799 Sun, D.-Z., and R. S. Lindzen, 1993: Distribution of tropical tropospheric water vapors. *J. Atmos.*
800 *Sci.*, **50**, 1643–1660, doi:10.1175/1520-0469(1993)050<1643:DOTTWV>2.0.CO;2.
- 801 Trenberth, K. E., 1998: Atmospheric moisture residence times and cycling: Implications for
802 rainfall rates and climate change. *Climatic Change*, **39**, 667–694.
- 803 Wall, C. J., and D. L. Hartmann, 2015: On the influence of poleward jet shift on shortwave cloud
804 feedback in global climate models. *J. Adv. Model. Earth Syst.*, **7**, doi:10.1002/2015MS000520.
- 805 Wu, P., B. Xi, X. Dong, and Z. Zhang, 2018: Evaluation of autoconversion and accre-
806 tion enhancement factors in general circulation model warm-rain parameterizations using
807 ground-based measurements over the Azores. *Atmos. Chem. Phys.*, **18**, 17 405–17 420, doi:
808 10.5194/acp-18-17405-2018.
- 809 Yang, H., and R. T. Pierrehumbert, 1994: Production of dry air by isentropic mixing. *J. Atmos.*
810 *Sci.*, **51**, 3437–3454, doi:0.1175/1520-0469(1994)051<3437:PODABI>2.0.CO;2.
- 811 Zhao, M., 2014: An investigation of the connections among convection, clouds, and climate
812 sensitivity in a global climate model. *J. Climate*, **27**, 1845–1862, doi:10.1175/JCLI-D-13-00145.
813 1.
- 814 Zhao, M., I. M. Held, S.-J. Lin, and G. A. Vecchi, 2009: Simulations of global hurricane climatol-
815 ogy, interannual variability, and response to global warming using a 50-km resolution GCM. *J.*
816 *Climate*, **22**, 6653–6678, doi:10.1175/2009JCLI3049.1.

817 **LIST OF TABLES**

818 **Table 1.** Description of the experiments. 39

819 **Table 2.** Summary of STET (15°-90°) precipitation variables: average precipitation (P)
820 and evaporation (E); condensation (CE), formation (FE), sedimentation (SE),
821 and precipitation (PE) efficiencies; residence time (RT). See text for definition
822 of these variables. 40

TABLE 1. Description of the experiments.

Name	Description
Base	control simulation with specific humidity tracer and saturation adjustment
Cloud	control simulation with specific humidity and cloud tracers (liquid, ice, and fraction) and microphysics
RHc100	variant of Cloud simulation requiring 100% grid-box-mean RH for cloud formation (RH_c)
noRESS	variant of Cloud simulation without rain evaporation or snow sublimation
halvAUTO	variant of Cloud simulation halving the raw computed value for autoconversion at each time-step
doubAUTO	as halvAUTO, but doubling, instead of halving, autoconversion
RHc100_noRESS	variant of Cloud simulation combining both RHc100 and noRESS variations

823 TABLE 2. Summary of STET (15°-90°) precipitation variables: average precipitation (P) and evaporation (E);
 824 condensation (CE), formation (FE), sedimentation (SE), and precipitation (PE) efficiencies; residence time (RT).
 825 See text for definition of these variables.

run	P	E	CE	FE	SE	PE	RT
	mm day ⁻¹		%				days
Base	1.84	2.34	78.5	–	–	–	13.1
Cloud	1.91	2.37	83.9	98.2	79.7	78.3	12.7
RHc100	1.71	2.17	81.2	95.2	89.4	85.1	14.3
noRESS	2.00	2.47	81.3	97.9	100.	97.9	11.8
halvAUTO	1.84	2.31	83.6	97.6	79.8	77.9	13.1
doubAUTO	1.98	2.44	84.3	98.6	79.6	78.5	12.2

826 **LIST OF FIGURES**

827 **Fig. 1.** Comparison of zonally-averaged, column-integrated WV, CC, and precipitation (P) ten-
828 dency terms in control cases (black totals, blue sources, and red sinks). Cloud case terms
829 (depicted as indicated by the legends) shown are (a) total (WV), surface evaporation (Ev),
830 rain evaporation (RE), snow sublimation (SS), and net condensation (Co); (b) total (CC),
831 net condensation (Co), autoconversion (Au), accretion (Ac), and ice settling (IS); (c) total
832 (P), net formation (Form), net sinks (RESS), and moisture convergence (P-E, surface precip-
833 itation minus evaporation). Base case terms (depicted as half-width lines) shown are total
834 WV, surface evaporation, saturation adjustment as net condensation in (a) and precipitation
835 in (c), and saturation adjustment minus evaporation as P-E in (c). Units are $10^{-6} \text{ kg m}^{-2} \text{ s}^{-1}$.
836 A positive tendency value denotes (a) WV, (b) CC, or (c) precipitation increasing. Totals
837 include the less significant tendency terms not shown individually. 43

838 **Fig. 2.** Principal WV and CC sources and sinks for various model runs (see Table 1) represented as
839 column-integrated average STET (15° - 90°) tendency values. For clarity, the smallest terms
840 are conglomerated in an other (O) category. Processes shown are WV sources: surface
841 evaporation (Ev), rain evaporation (RE), and snow sublimation (SS); WV sink (CC source):
842 LS condensation (Co); CC sinks: autoconversion (Au), accretion (Ac), and ice settling (IS).
843 Base case saturation adjustment is labeled LS condensation. Tendency units (vertical axis)
844 are $10^{-6} \text{ kg m}^{-2} \text{ s}^{-1}$. Percentages are given with respect to total source or sink category and
845 may not add to 100% due to rounding. 44

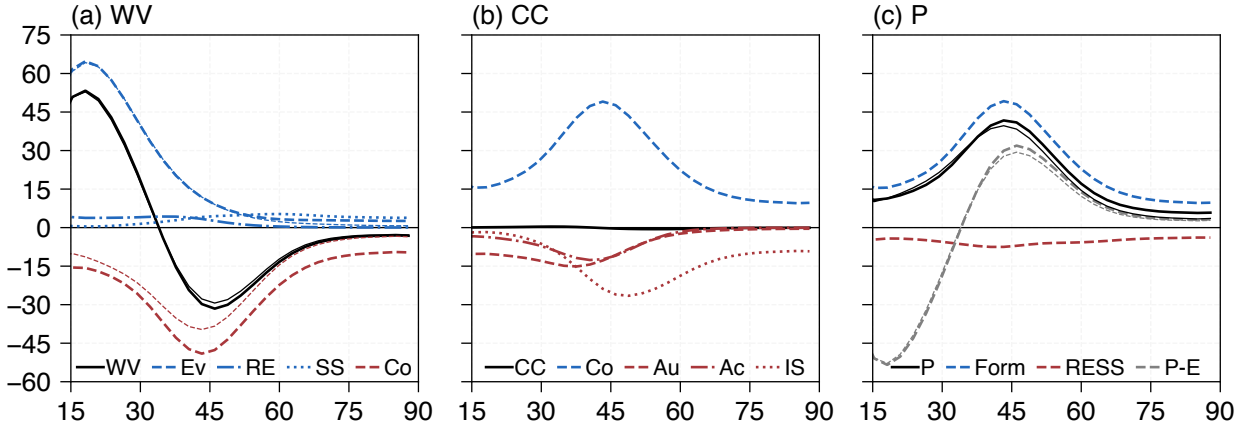
846 **Fig. 3.** Diagram of the water cycle in the control cloud microphysics scheme (Cloud experiment).
847 Water is cycled between four species (reservoirs): WV, CC, precipitation, and an assumed
848 surface reservoir. The quantities shown are average STET (15° - 90°) tendency values with
849 units of $10^{-6} \text{ kg m}^{-2} \text{ s}^{-1}$. Each reservoir shows either a balance (0.0) or an imbalance. Here,
850 condensation comprises both LS condensation and deposition; evaporation comprises both
851 LS evaporation and sublimation; formation includes autoconversion, accretion, ice settling,
852 and melting of cloud ice to rain; and sedimentation represents formation processes minus
853 RESS. 45

854 **Fig. 4.** Key variables in control runs: (a) RH difference (Cloud minus Base, %) as shading and
855 Base RH as contours (5% spacing), (b) temperature (K) as shading and potential temperature
856 as contours (5K spacing), (c) Cloud CF (%) as shading and Cloud RH as contours (5%
857 spacing), (d) Cloud total CC ($10^{-6} \text{ kg kg}^{-1}$) as shading and liquid (solid) and ice (dashed)
858 CC as contours (5 $10^{-6} \text{ kg kg}^{-1}$ spacing). Variables have been zonally averaged, and the x-
859 and y-axes are latitude and pressure (hPa), respectively. 46

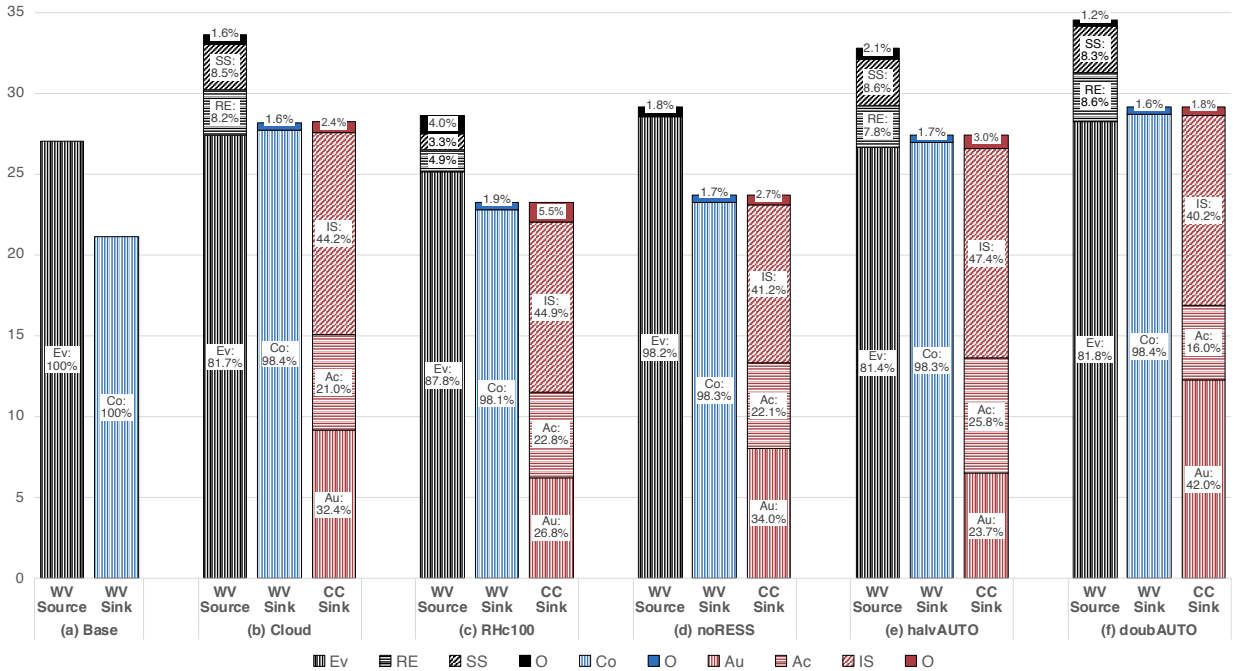
860 **Fig. 5.** Key variable changes in RHc100 perturbation from Cloud control: absolute differences in
861 zonally averaged (a) WV, (b) CC, and (c) precipitation (P) tendency terms (y-axis units of
862 $10^{-6} \text{ kg m}^{-2} \text{ s}^{-1}$); absolute differences in (d) RH, (e) CF, and (f) CC as shading with Cloud
863 case values as contours (5%, 5%, and 5 $10^{-6} \text{ kg kg}^{-1}$ spacing, respectively); comparison
864 of normalized histograms of (g) RH and (h) CF in Cloud (black) and RHc100 (grey) cases
865 from daily data (x-axis units of %) between 15° and 90° and 850 and 250 hPa with the y-axis
866 cut off at 0.15. For (a)-(c), WV, CC, and precipitation (P) tendency difference terms shown
867 are as defined in Fig. 1, with units of $10^{-6} \text{ kg m}^{-2} \text{ s}^{-1}$ where a positive tendency difference
868 denotes an increase in a WV/CC/P-increasing process or a decrease in a WV/CC/P-decreasing
869 process. For (a)-(f) variables have been zonally averaged and the x-axis is latitude; for (d-f)
870 the y-axis is pressure (hPa). For (g)-(h), histogram bins have widths of 5% and are all
871 half-open except for the last bin: [0, 5), [5, 10), ..., [100, 105]. 47

872 **Fig. 6.** As Fig. 5, but for noRESS perturbation. 48

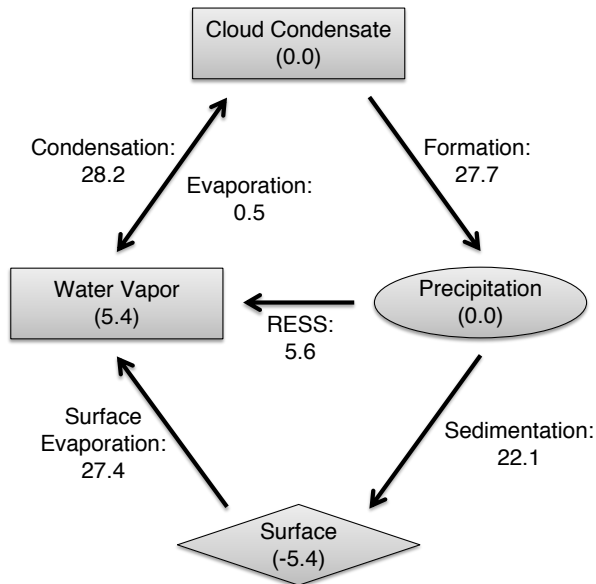
873	Fig. 7.	As Figs. 5 and 6, but for halvAUTO perturbation, except that the colorbar scale is reduced	
874		by a factor of 10 for (d) and (e).	49
875	Fig. 8.	Comparison of absolute RH differences (%) between control cases and intermediate setups:	
876		(a) RHc100 plus noRESS minus RHc100_noRESS minus Cloud [linearity check: should be	
877		0 if $RH_c = 83.3\%$ and RESS effects sum linearly], (b) RHc100_noRESS minus Base [CC	
878		advection effect] as shading, (c) noRESS minus RHc100_noRESS [$RH_c = 83.3\%$ effect] as	
879		shading, (d) noRESS minus Base [RESS effect] as color shading. All contours are Cloud	
880		minus Base difference with a spacing of 1%.	50



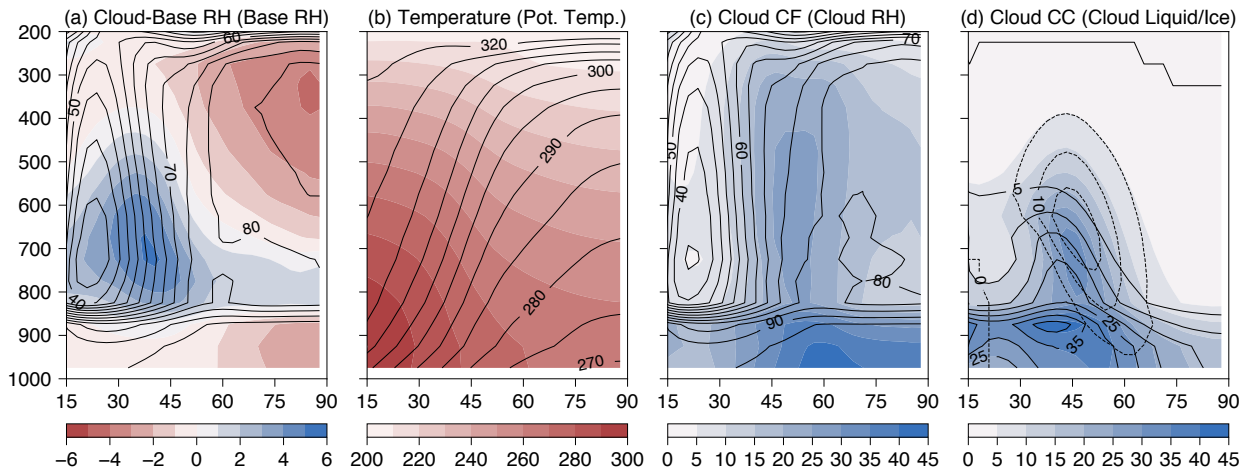
881 FIG. 1. Comparison of zonally-averaged, column-integrated WV, CC, and precipitation (P) tendency terms
 882 in control cases (black totals, blue sources, and red sinks). Cloud case terms (depicted as indicated by the
 883 legends) shown are (a) total (WV), surface evaporation (Ev), rain evaporation (RE), snow sublimation (SS),
 884 and net condensation (Co); (b) total (CC), net condensation (Co), autoconversion (Au), accretion (Ac), and
 885 ice settling (IS); (c) total (P), net formation (Form), net sinks (RESS), and moisture convergence (P-E, surface
 886 precipitation minus evaporation). Base case terms (depicted as half-width lines) shown are total WV, surface
 887 evaporation, saturation adjustment as net condensation in (a) and precipitation in (c), and saturation adjustment
 888 minus evaporation as P-E in (c). Units are $10^{-6} \text{ kg m}^{-2} \text{ s}^{-1}$. A positive tendency value denotes (a) WV, (b) CC,
 889 or (c) precipitation increasing. Totals include the less significant tendency terms not shown individually.



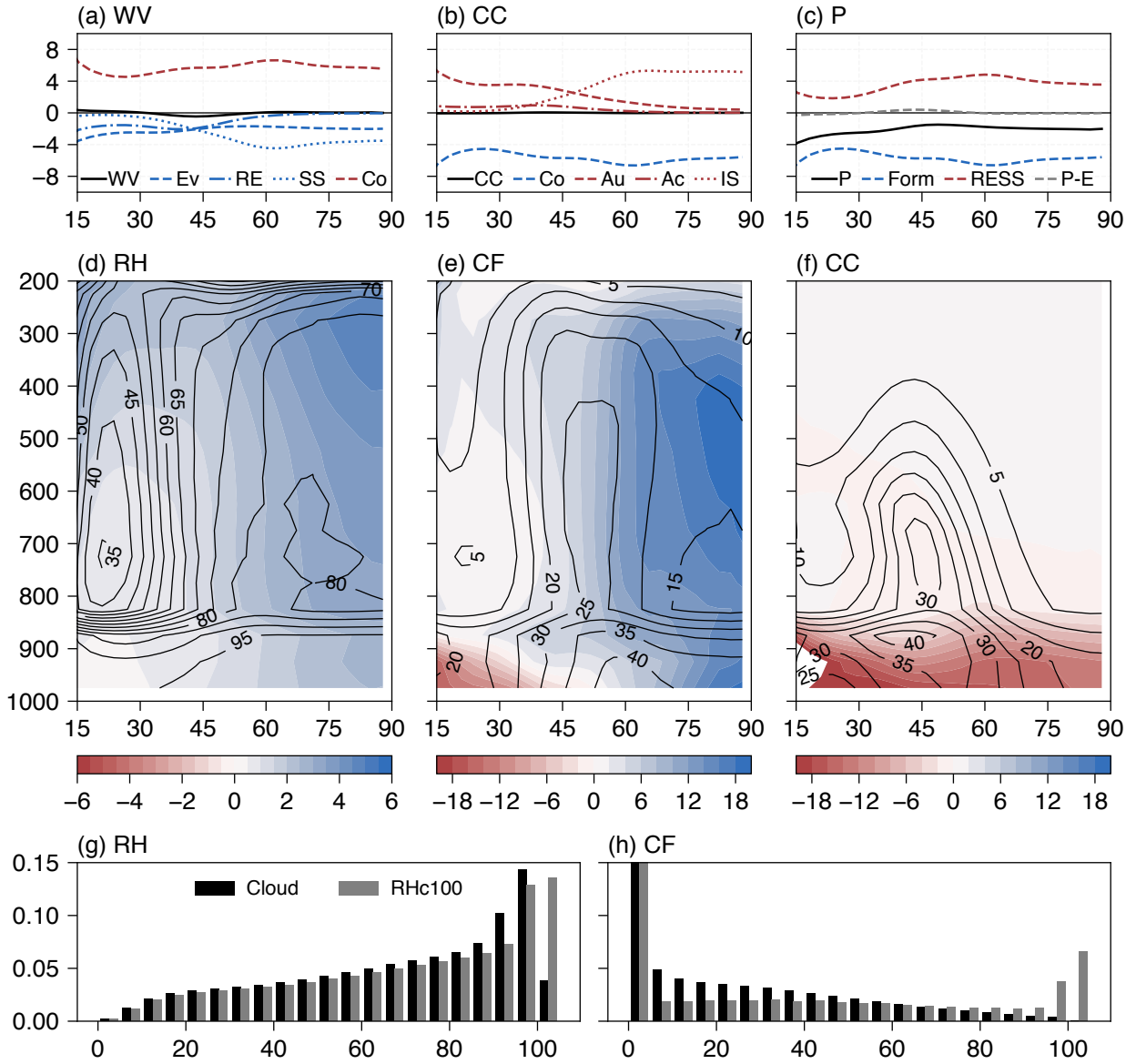
890 FIG. 2. Principal WV and CC sources and sinks for various model runs (see Table 1) represented as column-
 891 integrated average STET (15° - 90°) tendency values. For clarity, the smallest terms are conglomerated in an
 892 other (O) category. Processes shown are WV sources: surface evaporation (Ev), rain evaporation (RE), and
 893 snow sublimation (SS); WV sink (CC source): LS condensation (Co); CC sinks: autoconversion (Au), accretion
 894 (Ac), and ice settling (IS). Base case saturation adjustment is labeled LS condensation. Tendency units (vertical
 895 axis) are $10^{-6} \text{ kg m}^{-2} \text{ s}^{-1}$. Percentages are given with respect to total source or sink category and may not add
 896 to 100% due to rounding.



897 FIG. 3. Diagram of the water cycle in the control cloud microphysics scheme (Cloud experiment). Water is
 898 cycled between four species (reservoirs): WV, CC, precipitation, and an assumed surface reservoir. The quantities
 899 shown are average STET (15°-90°) tendency values with units of $10^{-6} \text{ kg m}^{-2} \text{ s}^{-1}$. Each reservoir shows either a
 900 balance (0.0) or an imbalance. Here, condensation comprises both LS condensation and deposition; evaporation
 901 comprises both LS evaporation and sublimation; formation includes autoconversion, accretion, ice settling, and
 902 melting of cloud ice to rain; and sedimentation represents formation processes minus RESS.



903 FIG. 4. Key variables in control runs: (a) RH difference (Cloud minus Base, %) as shading and Base RH
 904 as contours (5% spacing), (b) temperature (K) as shading and potential temperature as contours (5K spacing),
 905 (c) Cloud CF (%) as shading and Cloud RH as contours (5% spacing), (d) Cloud total CC ($10^{-6} \text{ kg kg}^{-1}$) as
 906 shading and liquid (solid) and ice (dashed) CC as contours ($5 \times 10^{-6} \text{ kg kg}^{-1}$ spacing). Variables have been zonally
 907 averaged, and the x- and y-axes are latitude and pressure (hPa), respectively.



908 FIG. 5. Key variable changes in RHc100 perturbation from Cloud control: absolute differences in zonally
 909 averaged (a) WV, (b) CC, and (c) precipitation (P) tendency terms (y-axis units of $10^{-6} \text{ kg m}^{-2} \text{ s}^{-1}$); absolute
 910 differences in (d) RH, (e) CF, and (f) CC as shading with Cloud case values as contours (5%, 5%, and $5 \cdot 10^{-6}$
 911 kg kg^{-1} spacing, respectively); comparison of normalized histograms of (g) RH and (h) CF in Cloud (black)
 912 and RHc100 (grey) cases from daily data (x-axis units of %) between 15° and 90° and 850 and 250 hPa with
 913 the y-axis cut off at 0.15. For (a)-(c), WV, CC, and precipitation (P) tendency difference terms shown are as
 914 defined in Fig. 1, with units of $10^{-6} \text{ kg m}^{-2} \text{ s}^{-1}$ where a positive tendency difference denotes an increase in a
 915 WV/CC/P-increasing process or a decrease in a WV/CC/P-decreasing process. For (a)-(f) variables have been
 916 zonally averaged and the x-axis is latitude; for (d-f) the y-axis is pressure (hPa). For (g)-(h), histogram bins have
 917 widths of 5% and are all half-open except for the last bin: $[0, 5)$, $[5, 10)$, ..., $[100, 105]$.

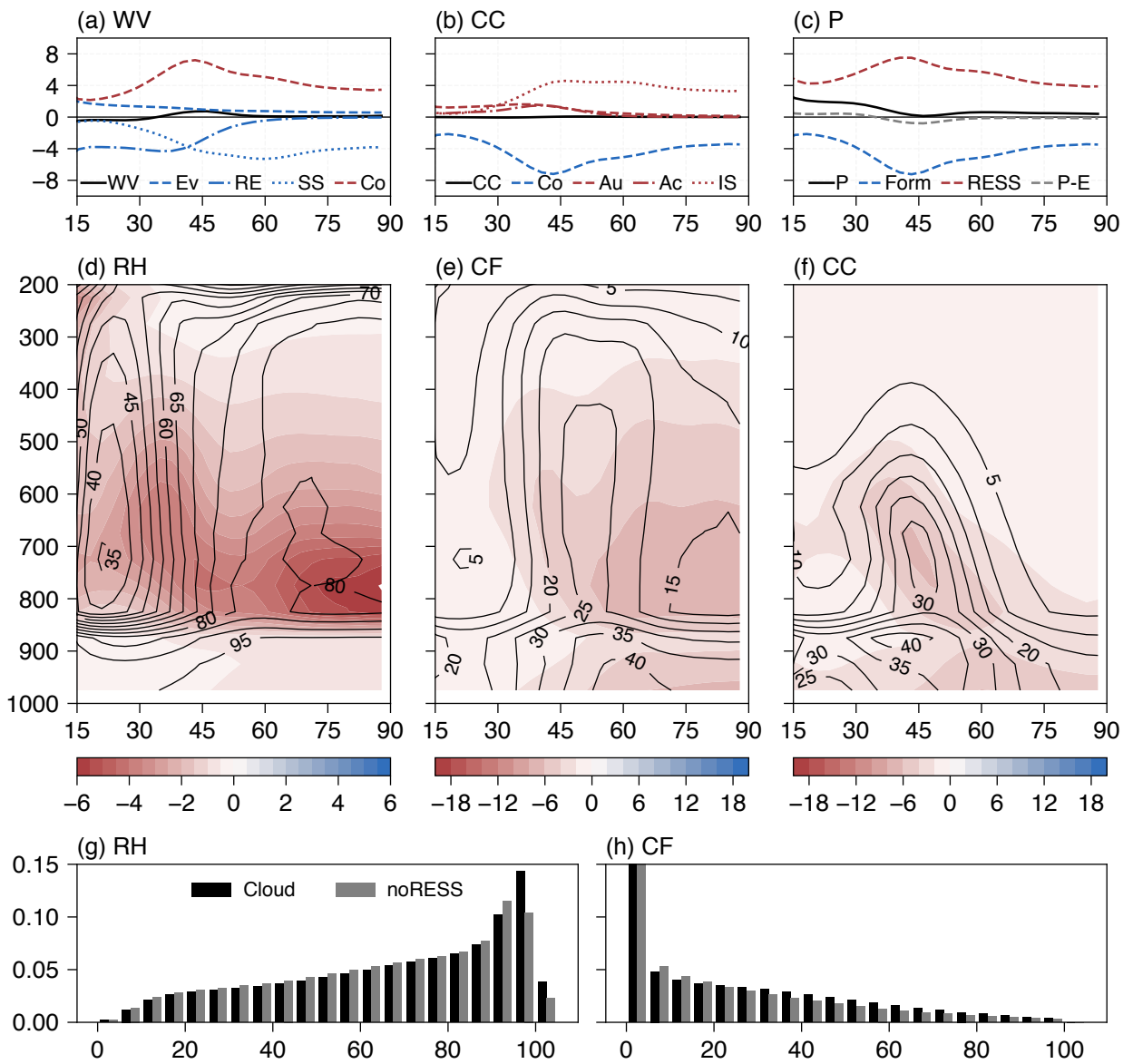
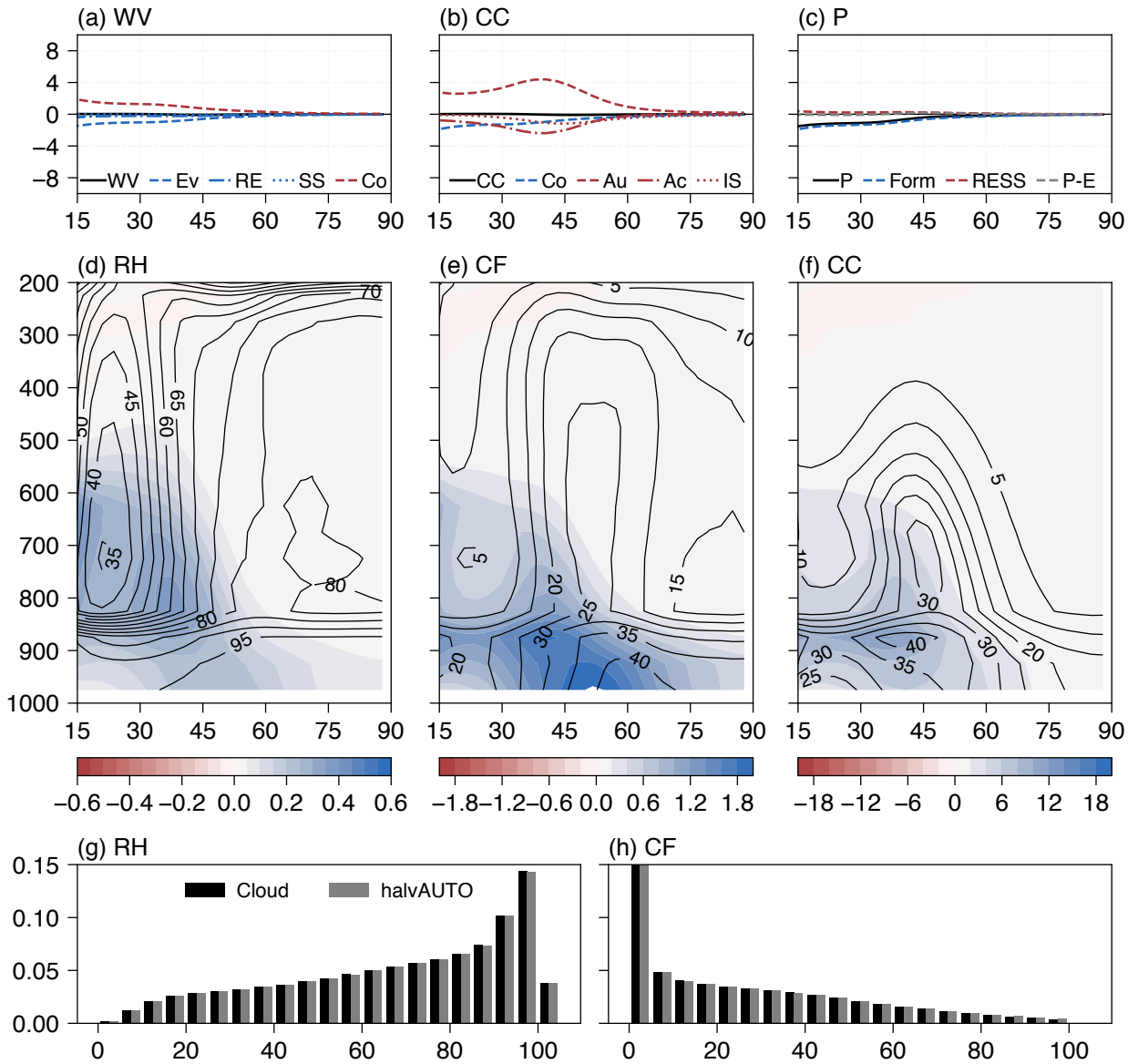
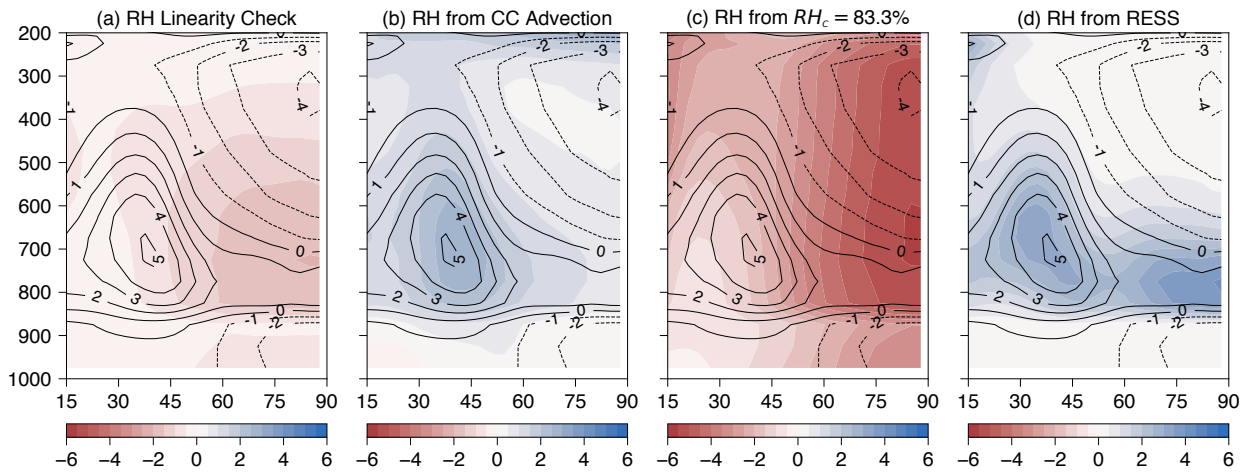


FIG. 6. As Fig. 5, but for noRESS perturbation.



918 FIG. 7. As Figs. 5 and 6, but for halvAUTO perturbation, except that the colorbar scale is reduced by a factor
 919 of 10 for (d) and (e).



920 FIG. 8. Comparison of absolute RH differences (%) between control cases and intermediate setups: (a) RHc100
 921 plus noRESS minus RHc100_noRESS minus Cloud [linearity check: should be 0 if $RH_c = 83.3\%$ and RESS
 922 effects sum linearly], (b) RHc100_noRESS minus Base [CC advection effect] as shading, (c) noRESS minus
 923 RHc100_noRESS [$RH_c = 83.3\%$ effect] as shading, (d) noRESS minus Base [RESS effect] as color shading.
 924 All contours are Cloud minus Base difference with a spacing of 1%.